Reaction of the Ethyl Radical with Oxygen at Millitorr Pressures at 243-368 K and a Study of the Cl + HO_2, Ethyl + HO_2, and HO_2 + HO_2 Reactions

Otto Dobis and Sidney W. Benson*

Contribution from Loker Hydrocarbon Research Institute, University of Southern California, University Park. Los Angeles, California 90089-1661

Received January 28, 1993. Revised Manuscript Received April 28, 1993®

Abstract: Ethyl radicals formed in the reaction of C_2H_6 + Cl are allowed to react with molecular oxygen in a very low pressure reactor (VLPR) experimental flow system over the temperature range of 243-368 K. Mass spectrometric analysis of reactants and products made possible the determination of rate constants (cm^3/(molecule·s)) of all major reaction steps. Mass balances for C, H, and Cl are good to ±4% on average. The elementary steps are the following: $C_2H_5 + O_2 \rightarrow HO_2 + C_2H_4$, $k_6 = (1.42 \pm 0.38) \times 10^{-17} \exp[(5064 \pm 154)/RT]$, measured independently from recording C_2H_5 consumption or C_2H_4 formation rates; $2HO_2 \rightarrow H_2O_2$, $k_7 = (4.50 \pm 0.56) \times 10^{-13} \exp[(1064 \pm 77)/RT]$; $C_2H_5 + HO_2 \rightarrow H_2O_2 + C_2H_4$, $k_{8a} = (2.98 \pm 0.11) \times 10^{-12}$; Cl + $HO_2 \rightarrow$ HCl + O_2, $k_9 = (4.45 \pm 0.06) \times 10^{-11}$. Activation energies are given in cal/mol. Reactions 8a and 9 show no change in the temperature range of measurements, while reactions 6 and 7 both have negative temperature dependence. The radical oxidation reaction 6 is suggested to occur via excited ethylperoxy and 2-hydroperoxyethyl radical formations as consecutive reversible steps.

Introduction

One of the most challenging subjects in chemical kinetics is the understanding of the oxidation of organic fuels at the molecular and radical levels. This process with many important practical applications is extremely complicated. It involves nearly all known principles of chemical kinetics, thermochemistry, and heat- and mass-transport phenomena. Direct experimental investigation of the overall combustion kinetics is not too revealing as the number of variables exceeds the number of parameters measurable simultaneously even in the early stages of what is a complex autocatalytic chain reaction system. Therefore, different stages of the overall process have been investigated in suitably designed experiments and the measured kinetic parameters of elementary steps have been assembled (usually with some simplifications) for computational modeling to obtain a "characteristic" model which describes satisfactorily the concentration, temperature, or pressure profiles of a real stage (e.g. the negative temperature coefficient for the slow oxidation and for cool flames).[1] However, this approach inherently raises questions as to how well the selected elementary rate constants mostly measured under isothermal conditions, as well as the chemical quasi-steady-state and partial equilibrium assumptions, fit in the time scale of a real system.[2] The scarcity of kinetic data on a number of important reaction steps makes it necessary to introduce reasonable estimates of some of the elementary reaction rates. When those rate constants are measured later on, the earlier model calculation often has to be remade.

Lately, important experimental investigations of low-pressure oxidation of methyl,[3] ethyl,[4] vinyl,[5] and 1-propenyl[6] radicals have provided some new insight into the slow combustion stage. Special interest is attached to ethyl radical oxidation, the fastest propagating step in flames, and its fast chain branching role in ignition.[7] At low temperature ($T < 420$ K), ethylperoxy radical unimolecular isomerization can only take place by one primary H atom intramolecular transfer through a 5-membered-ring TS.[8,9]

The most probable mechanism of ethyl radical oxidation at low temperature is

Scheme I

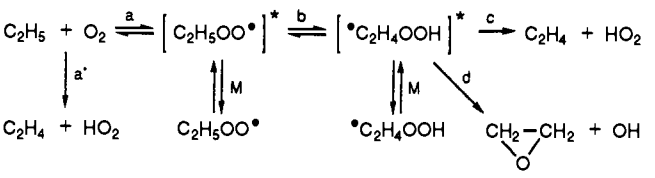

(an asterisk indicates an energized species)

Neither ethylene oxide nor OH are characteristic products of Scheme I at moderate pressure (>10 Torr), where the collisionally stabilized ethylperoxy radical concentration is significant and other reaction paths dominate. Instead, ethylene oxide can be produced[9] by reaction

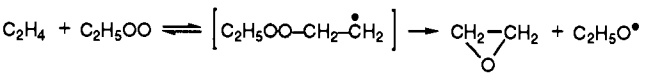

and, with excess O_2 at low temperature, OH radical may be produced[10] by the reaction sequence

$$C_2H_4OOH + O_2 \rightleftharpoons {}^{\bullet}OOC_2H_4OOH \rightleftharpoons HOOCH_2{}^{\bullet}CHOOH \rightarrow HO_2CH_2CHO + OH$$

At high temperature, HO_2CH_2CHO can further decompose,

® Abstract published in *Advance ACS Abstracts*, September 1, 1993.

(1) Griffiths, J. F.; Scott, S. K. *Prog. Energy Combust. Sci.* **1987**, *13*, 161.
(2) Dixon-Lewis, D. Computer Modeling of Combustion Reaction in Flowing System with Transport. In *Combustion Chemistry*; Gardiner, W. C., Jr., Ed. Springer-Verlag: New York, 1984; Chapter 2.
(3) Slagle, I. R.; Gutman, D. *J. Am. Chem. Soc.* **1985**, *107*, 5342.
(4) Wagner, B. F.; Slagle, I. R.; Sarzynsky, D.; Gutman, D. *J. Phys. Chem.* **1990**, *94*, 1853. Slagle, I. R.; Feng, Q.; Gutman, D. *Ibid.* **1984**, *88*, 3648.
(5) Slagle, I. R.; Park, J. Y.; Heaven, M. C.; Gutman, D. *J. Am. Chem. Soc.* **1984**, *106*, 4356.
(6) Slagle, I. R.; Park, J. Y.; Gutman, D. *Twentieth International Symposium on Combustion*; The Combustion Institute: Pittsburgh, 1985; p 733. Morgan, C. A.; Pilling, M. J.; Tulloch, J. M.; Ruiz, R. P.; Bayes, K. D. *J. Chem. Soc., Faraday Trans. 2* **1982**, *78*, 1323.
(7) Warnatz, J. Rate Coefficients in the C/H/O System. In *Combustion Chemistry*; Gardiner, W. C., Jr., Ed.; Springer-Verlag: New York, 1984; Chapter 3.
(8) Fish, A. Rearrangement and Cyclization Reactions of Organic Peroxy Radicals. In *Organic Peroxides*; Swern, D., Ed.; Wiley-Interscience: New York, 1970; Chapter 3.
(9) Benson, S. W. *J. Am. Chem. Soc.* **1965**, *87*, 972.
(10) Benson, S. W. *Prog. Energy Combust. Sci.* **1981**, *7*, 125.

0002-7863/93/1515-8798$04.00/0

producing one more OH together with $^{\bullet}OCH_2CHO$ which can rapidly decompose into $CH_2O + CHO$.

Scheme I illustrates the significance of collisional deactivation of two hot intermediates in the stepwise formation of C_2H_5OO and its decomposition into $C_2H_4 + HO_2$. Isomerization step b proceeds through a five-membered-ring TS with internal H atom transfer. Unimolecular steps b and c have appreciable activation energies and both are endothermic although the overall reaction a + b + c is 12 kcal exothermic. All these point to the key role of pressure in C_2H_5OO and HO_2 radical distributions. The slow oxidation outside the cool flame region is the regime of organic hydroperoxide production up to a critical concentration of RO_2H. The main source of RO_2H is the termination step[11]

$$RO_2 + HO_2 \rightarrow RO_2H + O_2$$

These and similar steps are also important in atmospheric chemistry.[12]

Experimental investigations of ethyl radical oxidation at low temperature have been carried out in the pressure range 1–8[4] and 0.6–10.5 Torr,[13] both using absolute rate measurements, in the range 3–1500 Torr[14] with a relative rate technique, and at 700 Torr.[15] The measured C_2H_4 yield varies from 16% at 0.6 Torr to about 0.01% at 1500 Torr, indicating that the collisional stabilization at step a is favored even at a pressure of 0.6 Torr and the process of C_2H_4 formation is rather close to its high pressure limit. It is also observed that the walls of an uncoated glass reactor enhance the stabilization of C_2H_5OO, reducing the C_2H_4 yield by a factor of 2 compared with a wall-coated reactor.[16] RRKM calculations with their multiparameter requirements are too flexible to give an accurate description of the fall-off region based on those data. For this purpose, kinetic data obtained at lower pressure are needed.

Ab inito calculations[17] show that the energy differences between six conformers of C_2H_5OO radical may be as high as 8 kcal/mol. The highest value belongs to the in-plane cis conformer, the precursor of the cyclic TS needed for C_2H_4OOH production. This may account for a part of the relatively high activation energy of step b which has been estimated at about 28 kcal/mol.

Scheme I becomes much simpler as $M \rightarrow 0$, and this is well suited to the technique of the very low pressure reactor (VLPR). In principle, it makes it possible to identify each barrier E_b^* and E_c^* in Scheme I.

Earlier, we reported[18] our results of the kinetic invesitgation of the $C_2H_6 + Cl$ reaction in the VLPR system which proved to provide a well-regulated C_2H_5 radical source over a wide range of temperature. This reaction mechanism consists of the following consecutive elementary steps:

Scheme II

$$C_2H_6 + Cl \rightarrow HCl + C_2H_5 \quad (1)$$

$$Cl + C_2H_5 \rightarrow HCl + C_2H_4 \quad (2)$$

$$2C_2H_5 \rightarrow C_2H_6 + C_2H_4 \quad (3)$$

$$C_2H_4 + Cl \rightleftharpoons HCl + C_2H_3 \quad (4)$$

$$C_2H_3 + Cl \rightarrow HCl + C_2H_2 \quad (5)$$

All five rate constants and their temperature dependences are known from earlier VLPR measurements.[18]

On introducing O_2 flow into the system, the mass signal of C_2H_5 decreases due to the radical consumption in oxidation, but the C_2H_6 signal also decreases indicating, as expected, that the ethane feedback reaction 3 is partly suppressed. The C_2H_4 signal increases and signals at mass 33 and 34 appear in excess over those from the ^{17}O and ^{18}O isotope composition of O_2. A very small, but still measurable, increase in the Cl signal can also be detected, which indicates that although reaction 2 has decreased, the fastest Cl consuming process in the system is reaction 1. All these observations point to the existence of the following additional reactions:

Scheme III

$$C_2H_5 + O_2 \xrightarrow{k_6} HO_2 + C_2H_4 \quad (6)$$

$$2HO_2 \xrightarrow{k_7} H_2O_2 + O_2 \quad (7)$$

$$C_2H_5 + HO_2 \xrightarrow{k_{8a}} H_2O_2 + C_2H_4$$

$$\xrightarrow{k_{8b}} C_2H_6 + O_2 \quad (8)$$

$$Cl + HO_2 \xrightarrow{k_{9a}} HCl + O_2$$

$$\xrightarrow{k_{9b}} ClO + OH \quad (9)$$

Reaction 6 is relatively slow; therefore, a large excess of O_2 has to be used, thereby putting it in the pseudo-first-order reaction regime.

No mass signals of other products, in particular, of O atom containing products or intermediates could be observed. An especially intensive search was devoted to those of CH_3CHO, CH_2CH_2O, and C_2H_5O. Since $m/e = 44$ is the signal of CO_2 background, it sets the mass spectral detection limit of any mass 44 product specific loss rate to $(1.5 \pm 0.9) \times 10^{10}$ molecules/(cm^3·s). Depending on the escape orifice used (k_{eM}, s^{-1}), this corresponds to the range of steady state concentrations (0.5–2.0) $\times 10^{10}$ molecules/cm^3. The background signal of $m/e = 45$ is about 5 times less than that at 44 amu. It sets the flow detection limit at 45 amu to $(3.6 \pm 3.2) \times 10^9$ molecules/(cm^3·s), which corresponds to the range of $(1.0–4.9) \times 10^9$ molecules/cm^3 in steady state concentrations.

In the present study we report on the kinetic investigation of reactions 6–9 over the temperature range of 243–368 K. With appropriate changes in concentration of the initial components $(Cl)_0$, $(C_2H_6)_0$, and $(O_2)_0$, varying the residence time, and conducting overall mass spectrometric product analysis, it was possible to obtain rate constants for all four major steps of Scheme III. At the same time, mass balances between Cl and C_2H_6 consumptions and product formation were found in excellent agreement (±4%).

Experimental Section

The same "three-chamber" turbo-pumped apparatus described earlier[18,19] was used in the present study. It has a reactor cell with a volume (V_r) of 215.7 cm^3, its inner wall is thin-teflon coated, and the outer wall is enclosed in a heating–cooling jacket connected to either a NESLAB ULT-80DD refrigerated circulator or a HAAKE FS-2 constant temperature bath circulator. Its bottom opening is on a rapidly-adjustable slide[19] with three interchangeable discharge orifices of diameter 0.193, 0.277, and 0.485 cm denoted as Φ_2, Φ_3, and Φ_5, respectively. With this reactor volume, the escape rate constant for the unimolecular gas-dynamic process of

$$M \xrightarrow{k_{eM}} \text{escape from cell} \quad (e)$$

is given by $k_{eM} = a_\Phi(T/M)^{1/2}$, s^{-1}, where M is the mass of any individual gas component present in the reactor cell, T is the absolute temperature,

(11) Benson, S. W. *Twenty-First International Symposium on Combustion*; The Combustion Institute: Pittsburgh, 1986; p 703.
(12) Finlayson-Pitts, B. J.; Pitts, J. N. *Atmospheric Chemistry*; Wiley-Interscience: New York, 1986; pp 33 and 407.
(13) Plumb, J. C.; Ryan, K. R. *Int. J. Chem. Kinet.* **1981**, *13*, 1011.
(14) Kaiser, E. W.; Wallington, T. J.; Andino, J. M. *Chem. Phys. Lett.* **1990**, *168*, 309.
(15) Niki, H.; Maker, P. D.; Savage, C. M.; Breitenbach, L. P. *J. Phys. Chem.* **1982**, *86*, 3825.
(16) Kaiser, E. W.; Lorkovich, J. M.; Wallington, T. J. *J. Phys. Chem.* **1990**, *94*, 3352.
(17) Quelch, G. E.; Gallo, M. M.; Schaefer, H. F., III *J. Am. Chem. Soc.* **1992**, *114*, 8239.
(18) Dobis, O.; Benson, S. W. *J. Am. Chem. Soc.* **1991**, *113*, 6377. Dobis, O.; Benson, S. W. *Ibid.* **1990**, *112*, 1023.
(19) Dobis, O.; Benson, S. W. *Int. J. Chem. Kinet.* **1987**, *19*, 691.

Table I. Isotopic Contributions[a] to the Spectra of O_2 at 20- and at 40-eV Ionization Energies

V_i, V	$F(O_2)$, molecule/(cm³·s)	I_{16}, %	I_{33}, %	I_{34}, %
20	12.986	0.026 ± 0.021	0.074 ± 0.019	0.416 ± 0.057
40	12.986	3.882 ± 0.018	0.073 ± 0.012	0.419 ± 0.040
20	19.622	0.027 ± 0.017	0.075 ± 0.015	0.391 ± 0.065
40	19.622	4.000 ± 0.015	0.075 ± 0.008	0.404 ± 0.017
			av: 0.074 ± 0.013	0.408 ± 0.045

[a] Values given are $(I/\Sigma_k I_k) \times 100$ where $\Sigma_k I_k$ are the sum of all the mass signals from O_2.

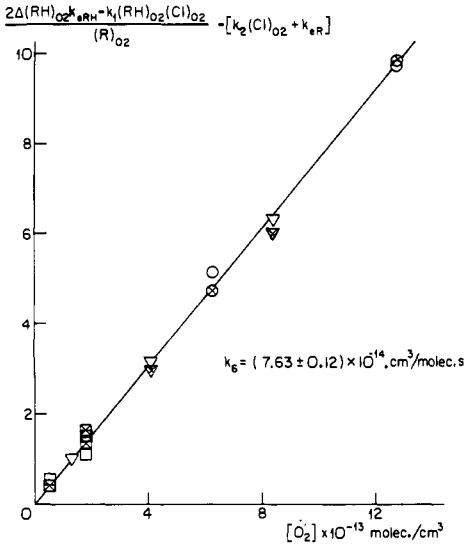

Figure 1. Dependence of ethyl radical consumption on oxygen concentration according to eq 12b with $\Delta k_8 = 0$ at 298 K. The slope gives k_6 directly. $k_1 = 6.1 \times 10^{-11}$ cm³/(molecule·s) and $k_2 = 1.2 \times 10^{-11}$ cm³/(molecule·s) are taken from ref 18. Symbols indicating the orifices used for the given data pairs: ○, ϕ_2; ▽, ϕ_3; □, ϕ_5. Crossed and open symbols represent the data obtained with 20- and 40-V ionizing electrons.

and $a_\Phi = 0.285$ for Φ_2, 0.546 for Φ_3, and 1.321 for Φ_5 orifices. The top of the cell is equipped with three inlet openings connected to different capillary flow subsystems used for regulated inlet flow of the initial components.

It is convenient for us to define a specific reaction flux (flux/V_r) of reactants (F(M), molecule/(cm³·s)) into the reactor vessel which can be calibrated by measuring the time dependence of the pressure drop of gas M flown from a buffer reservoir of known volume. The initial steady-state concentration of M in the reactor cell is than calculated from the following relation: $[M] = F(M)/k_{eM}$. Mass spectral calibrations are carried out by measuring absolute mass signal intensities (I_M) as a function of F(M) according to the relationship $(I_M) = \alpha_M F(M)$, where α_M is the mass spectral efficiency of M (see e.g. Figure 3 or 4) in our instrument.

First, the Cl atom flow was established with use of a 4.5% Cl_2/He mixture (both Matheson research grade gases) conducted through the microwave cavity of a McCarrol antenna before entering the reactor cell. The microwave power was adjusted to 100% break-up of Cl_2 and checked by the disappearance of the Cl_2 mass signal. Then, C_2H_6 flow (Matheson research-grade ethane) of a 4.90% C_2H_6/He mixture was started up and gradually increased until the Cl mass signal has been reduced to a small, but measurable, value. Finally, pure O_2 flow (Matheson research grade oxygen) was introduced and regulated until a sizable decrease in C_2H_5 mass signal has been achieved. At each step, all mass spectral data necessary for calculations according to kinetic equations were recorded with a BALZERS QMG 511 quadrupole mass spectrometer equipped with an off-axis mass analyzer. Mass scans in the parent mass area of expected side products were also carried out in each run.

Because of the coincidence of mass signals of O_2 isotopes with those of HO_2 and H_2O_2, it is essential to know the exact isotope composition of the oxygen gas used. It was checked by the mass signal distributions of O_2 recorded at two different gas flows, $F(O_2)$, using electron voltages of 20 V and 40 V (these two voltages are used in all experiments). The results are summarized in Table I together with the measured O^+ atom fragmentation ratio from O_2. The isotope distributions found are in excellent agreement with the standard natural abundance of oxygen isotopes (*CRC Handbook of Chemistry and Physics*, 73rd ed.; 1992–93, Section 11, p 30).

Results

When O_2 is absent, the steady-state concentration of the ethyl radical can be derived from the steady-state kinetics of reactions 1–3 and e given by

$$(R) = \frac{2\Delta(RH)k_{eRH} - k_1(RH)(Cl)}{k_2(Cl) + k_{eR}} \quad (10)$$

where $(R) = (C_2H_5)$, $\Delta(RH) = (C_2H_6)_0 - (C_2H_6)$, and k_{eRH} and k_{eR} are the first-order escape rate constants of RH and R.

With O_2 flow, the ethyl radical concentration drops to a lesser value due to reactions 6 and 8 of Scheme III:

$$(R)_{O2} = \frac{2\Delta(RH)_{O2}k_{eRH} - k_1(RH)_{O2}(Cl)_{O2}}{k_2(Cl)_{O2} + k_6(O2) + (\Delta k_8)(HO_2) + k_{eR}} \quad (11)$$

where index O2 denotes the steady-state concentration of a given reactant in the presence of O_2, $\Delta(RH)_{O2} = (RH)_0 - (RH)_{O2}$, and $\Delta k_8 = k_{8a} - k_{8b}$.

The ratio of eqs 10 and 11 leads to

$$k_6(O_2) + \Delta k_8(HO_2) = \left(\frac{2\Delta(RH)_{O2}k_{eRH} - k_1(RH)_{O2}(Cl)_{O2}}{2\Delta(RH)k_{eRH} - k_1(RH)(Cl)}\frac{(R)}{(R)_{O2}} - 1\right)[k_2(Cl) + k_{eR}] - k_2\Delta(Cl)' \quad (12a)$$

where $\Delta(Cl)' = (Cl)_{O2} - (Cl)$, a small positive change in Cl concentration which was observed in all experimental runs with O_2. An alternative rate equation can be obtained by rearranging eq 11 into

$$k_6(O_2) + \Delta k_8(HO_2) = \frac{2\Delta(RH)_{O2}k_{eRH} - k_1(RH)_{O2}(Cl)_{O2}}{(R)_{O2}} - [k_2(Cl)_{O2} + k_{eR}] \quad (12b)$$

The right sides of both eqs 12a and 12b contain concentration variables, all measurable in our experiments, and rate constants, all known from our earlier work,[18] so that either of them could be used for the determination of k_6 in principle. But k_8 is not known from experimental study. One estimate[20] gives a low value for k_{8a} ($\sim 5 \times 10^{-13}$ cm³/(molecule·s)) and suggests that $k_{8a} = k_{8b}$. However, in the following we will show that k_{8a} is about six times higher according to our experimental results, but $k_{8a} \simeq k_{8b}$ can be rationalized if disproportionation 8b produces triplet oxygen (O_2,³ Σ). It can definitely be stated that $k_8(HO_2) \ll k_6(O_2)$.

Neglecting $\Delta k_8(HO_2)$, k_6 was calculated according to both eqs 12a and 12b. Since small random deviations were found between them throughout the entire O_2 concentration range used, the results were averaged in pairs. Mass signals were recorded at both 20- and 40-V ion acceleration voltages. The results obtained at 298 K temperature are presented in Figure 1. Rate constant $k_6 = (7.63 \pm 0.12) \times 10^{-14}$ cm³/(molecule·s) relates to the ethyl radical consumption rate in reaction step 6. According to reaction Scheme I it may not necessarily be the same for the product formation rate and distribution. However, the same rate equation for C_2H_4 product formation can be derived from the steady-state equations for ethylene (VH), vinyl radical (V), and ethane:

(20) Tsang, W.; Hampson, R. F. *J. Phys. Chem. Ref. Data* **1986**, *15*, 1087.

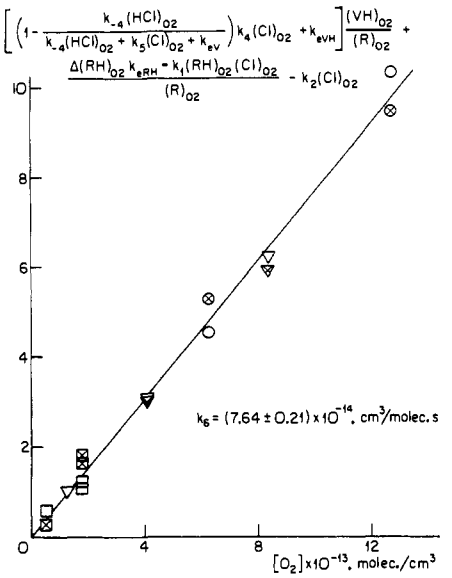

Figure 2. Dependence of ethylene production on oxygen concentration according to eq 13 with $\Delta k_8 = 0$ at 298 K. The slope gives k_6 directly. Symbol representations are the same as those in Figure 1.

$$k_6(O_2) + \Delta k_8(HO_2) = \left[\left(1 - \frac{k_{-4}(HCl)_{O2}}{k_{-4}(HCl)_{O2} + k_5(Cl)_{O2} + k_{eV}}\right)k_4(Cl)_{O2} + k_{eVH}\right] \times \frac{(VH)_{O2}}{(R)_{O2}} + \frac{\Delta(RH)_{O2}k_{eRH} - k_1(RH)_{O2}(Cl)_{O2}}{(R)_{O2}} - k_2(Cl)_{O2} \quad (13)$$

Again, the right side of eq 13 contains measured concentration parameters and known rate constants.[18] The expression in parentheses of the first term changes very little with chlorine concentration, but it varies rather with the changeover of orifice sizes. Neglecting $\Delta k_8(HO_2)$ and taking $k_5 = k_2$ (see ref 18), the results obtained at 298 K are plotted in Figure 2. The rate constant k_6 is found to be the same as before, but the scatter is almost doubled. The coincidence of rate constants obtained with reactant consumption or product formation rates discloses that in these experiments, where the overall pressure in the reactor cell varies from 0.45 to 4.7 mTorr, there is no formation of collisionally stabilized C_2H_5OO radicals and the oxidation proceeds entirely to ethylene product. All regular checking on the parent mass signal of C_2H_5OO, done in every run, turned out to be negative. This allows us to derive the formation rate of HO_2 and H_2O_2 from Scheme III.

Concentrations of HO_2 and H_2O_2 are related to the mass signal excesses at $m/e = 33$ and 34 over the isotopes of oxygen. In all runs, the mass signal of O_2 flow was also recorded at $m/e = 32$. The data obtained with different oxygen flow and at all temperatures are plotted in Figure 3 with 20- and 40-V ionization potentials. Mass signals obtained with the same O_2 flow in different runs were averaged. Figure 4 shows the fragmentation of O_2 into O^+ with the use of 40-V ionizing electrons. No such fragmentation was found at 20 V (Table I). With the slopes of these figures and the isotope distribution data of Table I, the isotope contribution of O_2 to the measured mass signals of HO_2 and H_2O_2 can be taken into account.

Mass 33 and 34 signals are always found to be higher than that of the isotope composition of O_2. Typical raw data from runs at 243 K are presented in Figures 5a,b and 6a,b with 20- and 40-V electron ionizing energies, respectively, where dotted lines mark the contributions arising from the given isotope of the oxygen molecule. Since the signals also depend on (Cl) and (C_2H_6) as well as on the residence time at a given temperature, no general trend can be expected from such a simplified plot. In all

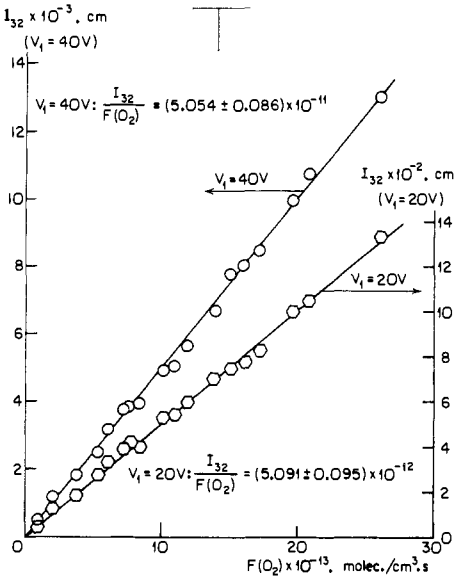

Figure 3. Mass 32 signal as a function of oxygen flow rate recorded with 20-V (hexagons; right ordinate) and 40-V (circles; left ordinate) ionizing electrons.

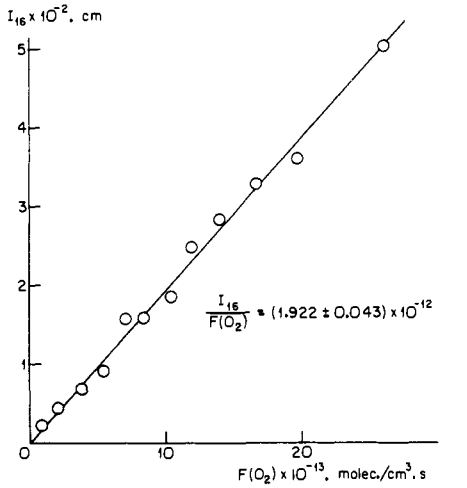

Figure 4. Mass 16 signal generated by O_2 fragmentation with 40-V ionizing electrons.

calculations ΔI_{33} and ΔI_{34} represent the mass signals at masses 33 and 34 minus the contribution due to O isotopes.

The steady-state conditions for HO_2 formation following from reactions 6–9 led to

$$k_{eHO2}(HO_2) = k_6(O_2)(R)_{O2} - 2k_7(HO_2)^2 - [(k_{8a} + k_{8b})(R)_{O2} + k_9(Cl)_{O2}](HO_2) \quad (14)$$

where $k_9 = k_{9a} + k_{9b}$. Similarly, the steady-state equation for H_2O_2 is obtained from reactions 7 and 8:

$$k_{eH2O2}(H_2O_2) = k_7(HO_2)^2 + k_{8a}(R)_{O2}(HO_2) \quad (15)$$

The combination of eqs 14 and 15 gives

$$\left(\frac{k_9(Cl)_{O2} - \Delta k_8(R)_{O2}}{k_{eHO2}} + 1\right)k_{eHO2}(HO_2) = k_6(O_2)(R)_{O2} - 2k_{eH2O2}(H_2O_2) \quad (16)$$

Taking $\Delta k_8 = 0$ and substituting the steady-state concentrations of H_2O_2 and HO_2 for their mass signal intensities gives

$$(H_2O_2) = \Delta I_{34}/\alpha_{34}k_{eHO2}$$

$$(HO_2) = \frac{\Delta I_{34}}{\alpha_{33}}\left(\frac{\Delta I_{33}}{\Delta I_{34}} - \frac{\beta_{33}}{\alpha_{34}}\right)\frac{1}{k_{eHO2}}$$

where α_{33} and α_{34} are the mass spectrometric efficiencies of HO_2

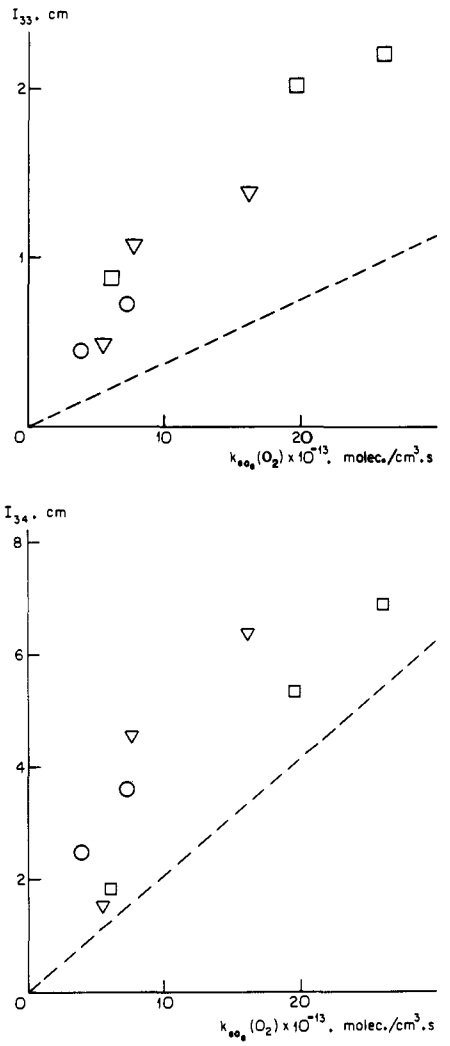

Figure 5. (a, top) Comparison of the mass 33 signal with the contribution from ^{16}O–^{17}O (dotted line) measured with 20-V ionizing electrons. Data points represent the recorded values of experiments at 243 K. Symbol representations are the same as in Figure 1. (b, bottom) The same as part a, but for the measured mass 34 signal with contribution from ^{16}O–^{18}O.

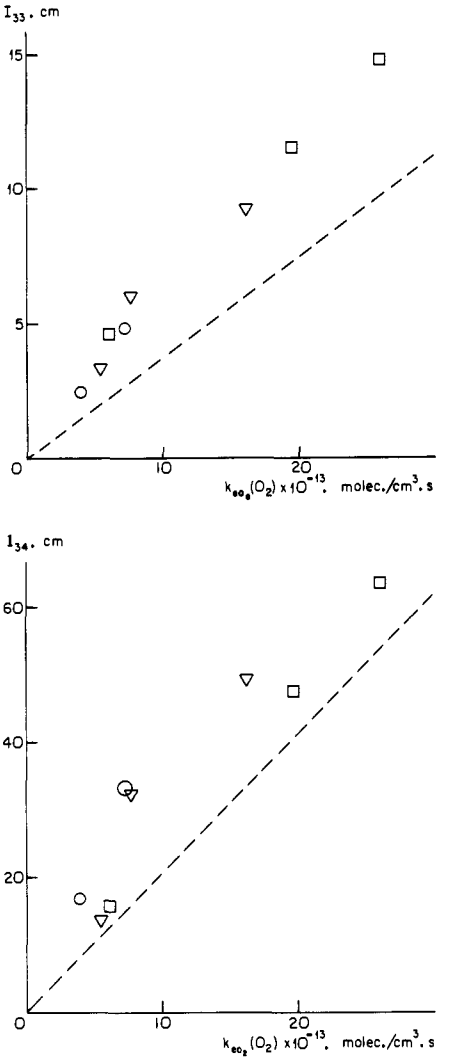

Figure 6. (a, top) Comparison of observed mass 33 signal with the contribution from ^{16}O–^{17}O (dotted line) measured with 40-V ionizing electrons. Data points represent the recorded values of experiments at 243 K. Symbol representations are the same as in Figure 1. (b, bottom) The same as part a, but for the measured mass 34 signal with contribution from ^{16}O–^{18}O.

and H_2O_2, respectively, and β_{33}/α_{34} is the fragmentation ratio of H_2O_2 into HO_2^+; eq 16 takes the form

$$\left(\frac{k_9(\mathrm{Cl})}{k_{\mathrm{eHO2}}}+1\right)\left(\frac{\Delta I_{33}}{\Delta I_{34}}-\frac{\beta_{33}}{\alpha_{34}}\right)=-2\frac{\alpha_{33}}{\alpha_{34}}+\alpha_{33}\frac{k_6(\mathrm{O_2})(\mathrm{R})_{\mathrm{O2}}}{\Delta I_{34}} \quad (16a)$$

In principle, α_{34} and β_{33}/α_{34} could be obtained from direct mass spectrometric calibration measurements of H_2O_2 flow, but it would have required a complete reconstruction of our flow capillary subsystem[21] where the surface-to-volume ratio is 175. The main problem is finding β_{33}/α_{34}. Once it is known α_{33} and α_{34} can be obtained from eq 16a. Note that besides the three concentration parameters (Cl, R and O_2), k_{eHO2} is also a variable of eq 16a which can be varied by a factor of 4.5 in three steps of orifice changeover.

An overview of our experimental data revealed that β_{33}/α_{34} must be very small, close to zero with 20-V ionization energy, but not with 40 V. It is evident that the flow rate ratio of HO_2 and H_2O_2

$$\frac{k_{\mathrm{eHO2}}(\mathrm{HO_2})}{k_{\mathrm{eH2O2}}(\mathrm{H_2O_2})}=\frac{\alpha_{34}}{\alpha_{33}}\left(\frac{\Delta I_{33}}{\Delta I_{34}}-\frac{\beta_{33}}{\alpha_{34}}\right) \quad (17)$$

must hold true regardless of whether 20- or 40-V electron energy is used for mass spectrometry. Taking $\beta_{33}/\alpha_{34} = 0$ at 20 eV, eq 17 gives a linear relationship for the two mass signal ratios measured with 40- and 20-V electron energies:

$$\left(\frac{\Delta I_{33}}{\Delta I_{34}}\right)_{40\mathrm{V}}=\left(\frac{\beta_{33}}{\alpha_{34}}\right)_{40\mathrm{V}}+\left(\frac{\alpha_{33}}{\alpha_{34}}\right)_{40\mathrm{V}}\left(\frac{\alpha_{34}}{\alpha_{33}}\right)_{20\mathrm{V}}\left(\frac{\Delta I_{33}}{\Delta I_{34}}\right)_{20\mathrm{V}} \quad (17a)$$

where the intercept is the fragmentation ratio at 40 eV. Plots of these data measured at all temperatures are shown in Figure 7, which gives $\beta_{33}/\alpha_{34} = (2.99 \pm 0.45) \times 10^{-2}$ for 40-V electron energy. This value is comparable with that of Foner and Hudson;[22] they found $\beta_{33}/\alpha_{34} = 0.045$ with 50-eV energy using a mass spectrometric setup similar to ours.

With $\beta_{33}/\alpha_{34} = 0.03$ for 40 eV and 0 for 20 eV, k_9 can be obtained by linear regression of eq 16a around the expected value of k_9. First it was done separately with data at each temperature.

(21) An attempt with pure unstabilized H_2O_2 (diluted to 1% with He) flow has resulted in complete decomposition according to the reaction $H_2O_2 = H_2O + {}^1/_2O_2$ in our flow capillary subsystem in full agreement with the known glass-surface catalyzed decomposition of H_2O_2; see e.g.: Schumb, W. C.; Satterfield, C. N.; Wentworth, R. L. *Hydrogen Peroxide*; Reinhold: New York, 1955; p 522.

(22) Foner, S. N.; Hudson, R. L. *J. Phys. chem.* **1962**, *36*, 2676.

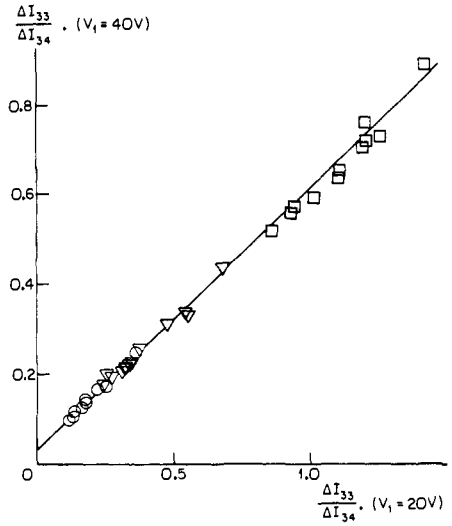

Figure 7. Mass signal ratios of HO_2 and H_2O_2 measured with 40-eV energy at all temperatures as a function of the same ratios measured with 20-eV energy plotted according to eq 17a. The intercept β_{33}/α_{34} = (2.99 0.45) × 10^{-2} is the fragmentation ratio at 40 eV. The slope is 0.578 ± 0.007. Symbol representations are the same as in Figure 1.

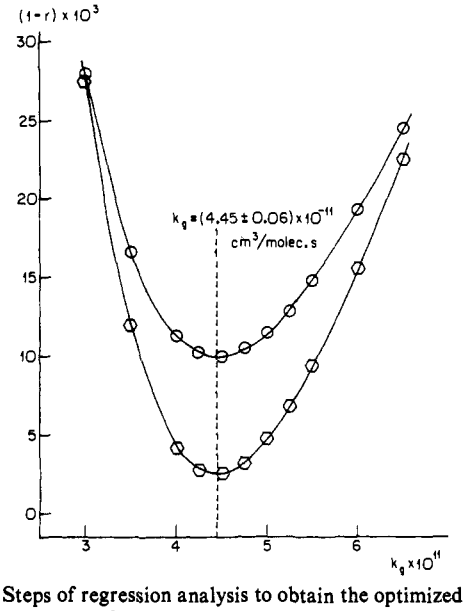

Figure 8. Steps of regression analysis to obtain the optimized value for k_9 according to eq 16a from the data series measured with 20-eV (circles) and 40-eV (hexagons) mass spectrometry. "r" is the regression coefficient.

The k_9 values were found to fall between 4.3 × 10^{-11} and 4.5 × 10^{-11} cm³/(molecule·s), without any definite trend with temperature. Therefore, we combined all related data and subjected them to regressional computation. The minima approached by marked regressional steps are shown in Figure 8 for both data series obtained with 20- and 40-eV mass spectrometry. The deeper minimum of the 40-eV data-set regression indicates that the mass analyses are more sensitive with 40 eV than with 20-eV mass spectrometry.

The best linear fit of data according to eq 16a, taking k_9 = (4.45 ± 0.06) × 10^{-11} cm³/(molecule·s) and β_{33}/α_{34} = 0, is presented in Figure 9a and gives α_{33} = (2.899 ± 0.075) × 10^{-12} for the slope and $2\alpha_{33}/\alpha_{34}$ = 0.262 ± 0.044 for the intercept with 20-eV energy mass spectrometry. The same type of linear fit is shown in Figure 9b taking β_{33}/α_{34} = 0.03 which gives α_{33} = (9.890 ± 0.208) × 10^{-12} for the slope and $2\alpha_{33}/\alpha_{34}$ = 0.156 ± 0.021 for the intercept with 40-eV energy mass spectrometry.

Rate constants k_7 and k_{8a} can be obtained from eq 15. Substituting the steady-state concentrations of H_2O_2 and HO_2 for their mass signal intensities in eq 15, after rearrangement, it

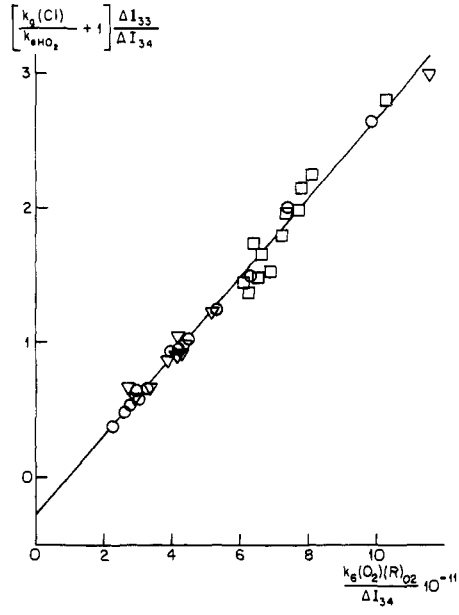

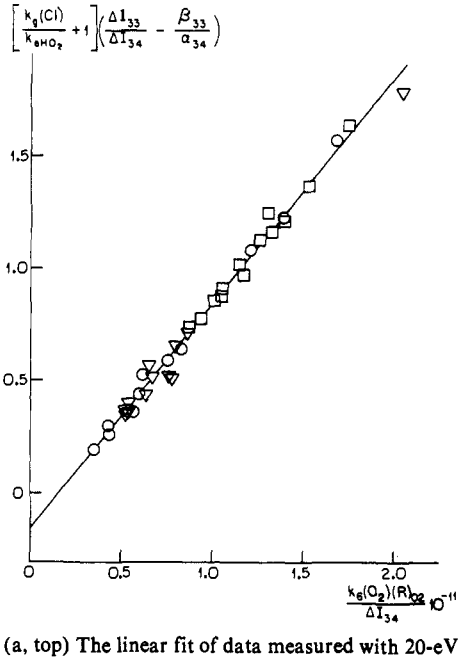

Figure 9. (a, top) The linear fit of data measured with 20-eV energy at all temperatures plotted according to eq 16a taking k_9 = 4.45 × 10^{-11} cm³/(molecule·s) (see Figure 8) and β_{33}/α_{34} = 0. Slope: α_{33} = (2.899 ± 0.075) × 10^{-12}. Intercept: $2\alpha_{33}/\alpha_{34}$ = 0.262 ± 0.044. Symbol representations are the same as in Figure 1. (b, bottom) The same linear fit as part a of data measured with 40-eV energy and taking β_{33}/α_{34} = 0.03. Slope: α_{33} = (9.890 ± 0.208) × 10^{-12}. Intercept: $2\alpha_{33}/\alpha_{34}$ = 0.156 ± 0.021.

becomes

$$\frac{k_{eHO2}}{(R)_{O2}}\left(\frac{\Delta I_{33}}{\Delta I_{34}}-\frac{\beta_{33}}{\alpha_{34}}\right)^{-1} = k_{8a}\frac{\alpha_{34}}{\alpha_{33}} + k_7\frac{\alpha_{34}}{\alpha_{33}^2}\left(\frac{\Delta I_{33}}{\Delta I_{34}}-\frac{\beta_{33}}{\alpha_{34}}\right)\frac{\Delta I_{34}}{k_{eHO2}(R)_{O2}} \quad (15a)$$

or with rearrangement

$$k_{eHO2}^2\left(\frac{\Delta I_{33}}{\Delta I_{34}}-\frac{\beta_{33}}{\alpha_{34}}\right)^{-2}\Delta I_{34}^{-1} = k_7\frac{\alpha_{34}}{\alpha_{33}^2} + k_{8a}\frac{\alpha_{34}}{\alpha_{33}}\left(\frac{\Delta I_{33}}{\Delta I_{34}}-\frac{\beta_{33}}{\alpha_{34}}\right)^{-1}\frac{k_{eHO2}(R)_{O2}}{\Delta I_{34}} \quad (15b)$$

With the known k_{eHO2} and measured (ΔI_{33}, ΔI_{34}, and the

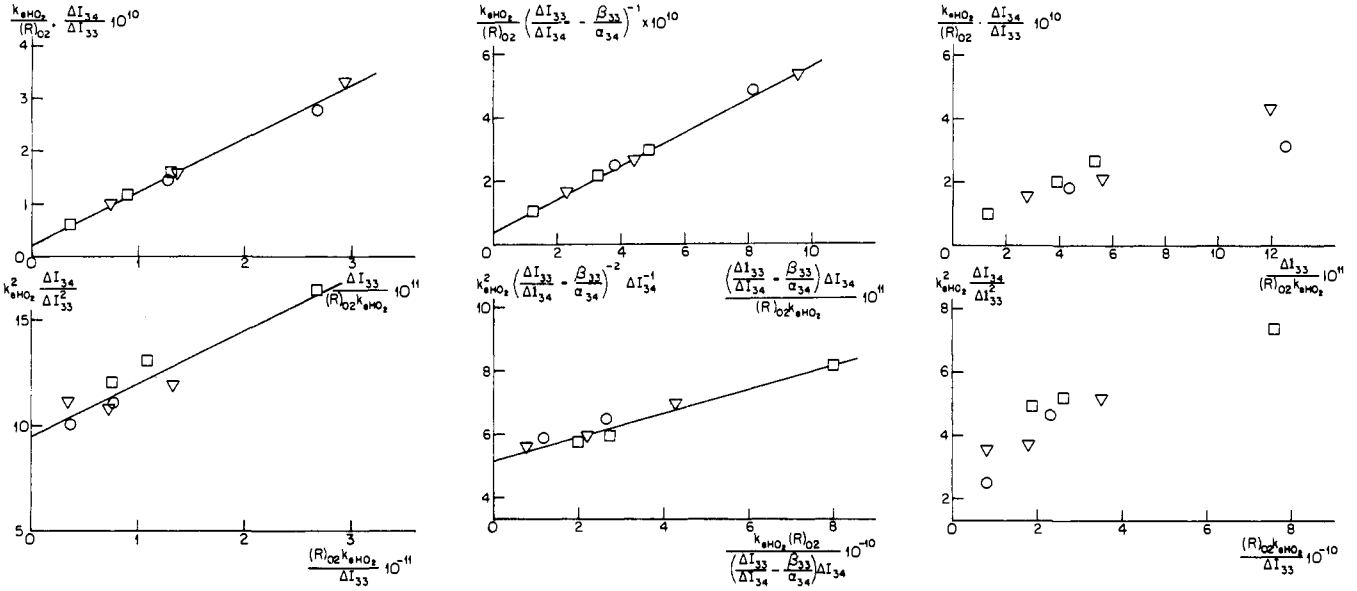

Figure 10. (a, left) The linear accommodation of kinetic parameters according to eq 15a, upper part, and eq 15b, lower part, with data measured with 20-eV energy ($\beta_{33}/\alpha_{34} = 0$) at 243 K. Upper line slope: 9.87 ± 0.40. Upper line intercept: (2.05 ± 0.42) × 10^{-11}. Lower line slope: 9.42 ± 0.48. Lower line intercept: (2.50 ± 0.39) × 10^{-11}. Symbol representations are the same as in Figure 1. (b, middle) The same as part a, but with data measured with 40-eV electron energy where $\beta_{33}/\alpha_{34} = 0.03$. Upper line slope: 5.28 ± 0.13. Upper line intercept: (3.57 ± 0.72) × 10^{-11}. Lower line slope: 5.20 ± 0.14. Lower line intercept: (3.78 ± 0.37) × 10^{-11}. (c, right) Illustration of the importance of $\beta_{33}/\alpha_{34} = 0.03$ for data evaluation with 40-eV electron energy. The same plot as part b, but with $\beta_{33}/\alpha_{34} = 0$.

Table II. Some Representative Analytical Data of Initial and Final Steady-State Concentrations over the Range of Temperatures and Residence Times Explored[a]

T, K	Φ_x[c]	$[Cl]_0$	$[C_2H_6]_0$	$[Cl]$	$[Cl_2H_6]$	$[C_2H_5]$	$[O_2]$	$[Cl]_{02}$	$\frac{[Cl]_{02}}{[Cl]_{02}+[H]_{02}}$	$[C_2H_6]_{02}$	$[C_2H_5]_{02}$	$[C_2H_4]_{02}$	$[HO_2]$	$[H_2O_2]$
243	Φ_2	14.17	11.20	0.386	3.94	3.37	495.4	0.810	0.0216	1.81	0.306	9.48	1.36	1.102
243	Φ_3	7.82	10.40	0.308	5.36	3.01	1084.8	0.525	0.0206	3.46	0.176	6.35	1.79	0.941
243	Φ_5	1.99	3.82	0.355	2.49	1.13	172.1	0.514	0.1030	2.12	0.483	1.14	0.614	0.067
268	Φ_2	13.71	9.70	0.618	2.22	2.96	974.2	0.901	0.0258	1.36	0.356	7.60	1.14	0.696
268	Φ_3	7.93	9.70	0.358	4.71	3.02	885.4	0.371	0.0234	4.14	0.482	4.87	1.78	0.833
268	Φ_5	1.86	3.27	0.393	2.09	1.04	160.5	0.491	0.1190	1.89	0.670	0.671	0.319	0.023[b]
298	Φ_2	12.14	11.69	0.308	4.55	3.30	1273.3	0.550	0.0162	2.49	0.710	8.06	1.52	1.115
298	Φ_3	5.23	6.09	0.385	2.82	2.10	411.5	0.567	0.0321	2.08	1.205	3.18	0.711	0.244
298	Φ_5	2.69	5.88	0.293	4.17	1.47	179.6	0.378	0.0841	3.83	1.332	0.659	0.146	0.010[b]
333	Φ_2	19.88	14.83	0.544	4.01	4.34	2843.0	0.935	0.0198	1.96	1.20	10.85	1.52	1.194
333	Φ_3	9.02	9.34	0.508	3.84	3.26	1403.0	0.645	0.0261	2.94	1.65	4.50	1.08	0.471
333	Φ_5	1.56	4.02	0.469	2.45	1.29	353.4	0.496	0.0955	2.37	1.11	0.496	0.157	0.153
368	Φ_2	15.35	15.24	0.324	6.00	4.17	1243.8	0.402	0.0122	4.44	3.09	7.30	1.116	1.309
368	Φ_3	6.07	9.25	0.301	4.43	3.70	755.6	0.456	0.0243	3.70	2.82	2.52	0.434	0.227
368	Φ_5	3.39	5.29	0.588	2.73	2.40	312.7	0.921	0.1402	2.40	1.92	0.902	0.084	~0.012[b]

[a] All concentrations are in units of 10^{11} particles/cm^3 taken as the average of 20- and 40-eV ionization energies of MS measurements. [b] H_2O_2 concentrations over ±50% uncertainty; they are not used in k_7, k_{8a}, and k_9 calculations. [c] Φ_x denotes the size of the escape orifice (see text).

concentration of R) variables, k_7 and k_{8a} can be obtained from the linearized form of either eq 15a or 15b as fitting constants at a given temperature multiplied by a combination of temperature independent mass spectrometric efficiencies (α_{33} and α_{34}) which are known from the former evaluation of eq 16a.

The linearity of eqs 15a and 15b is illustrated in parts a and b of Figure 10 using the measured data of experiments at 243 K. Figure 10a presents the accommodation of 20 eV of mass spectrometry ($\beta_{33}/\alpha_{34} = 0$) data measured according to eq 15a in the upper part and eq 15b in the lower part of the diagram. Figure 10b shows the same type of data accommodation with 40-eV mass spectrometry measurements where $\beta_{33}/\alpha_{34} = 0.03$. The average values of k_7 and k_{8a} calculated from the slopes and intercepts of these figures are given in the first row of the third and fourth columns of Table IV.

It may appear that the fragmentation ratio β_{33}/α_{34} at 40 eV is too small to affect the calculations, but it is not so. For illustration, the same functional presentation as Figure 10b is given in Figure 10c, but by taking $\beta_{33}/\alpha_{34} = 0$. It can be seen that eq 15a takes on a large scatter with great escape orifice size dependency, while eq 15b loses linearity due to the quadratic multiplicity term of the fragmentation ratio.

Experiments were carried out between 243 and 368 K in five steps. At each temperature step, all three initial reactant concentrations were varied, and the three different sizes of escape orifice were also used to change the residence time. These variations required 8–10 runs at each temperature. Moreover, each steady-state concentration measurement was taken from the average of 15–25 repeated mass scans made with both 20 and 40 eV. This resulted in a very large data accumulation. Some individual concentrations represented by various orifice sizes at different temperatures are listed in Table II. Since steady-state concentrations measured with 20- and 40-eV ionization energies differ slightly, they were actually averaged for rate constant calculations. The average values of those mass spectrometric concentration measurements are given in Table II. Concentrations of H_2O_2 and HO_2 are also listed. They can be calculated from measured ΔI_{34} and ΔI_{33} (corrected for β_{33} contribution) values along with known mass spectrometric efficiencies obtained from the evaluation of eq 16a.

The ranges of initial concentrations used and also of measured

Table III. Ranges of Initial and Final Steady-State Concentrations[a]

T, K	$[Cl]_0$	$[C_2H_6]_0$	$[O_2]$	$[Cl]_{02}$	$[C_2H_6]_{02}$	$[C_2H_5]_{02}$	$[C_2H_4]_{02}$	$[HO_2]$	$[H_2O_2]$	ΣP_i, mTorr
243	1.99–18.04	3.82–15.95	172.1–1769.5	0.387–1769.5	0.821–4.21	0.176–0.483	1.14–9.48	0.634–2.38	0.067–1.95	0.57–4.865
268	1.86–19.16	3.27–20.07	160.5–2382.5	0.369–1.45	1.22–4.39	0.238–0.760	0.67–13.63	0.389–3.05	0.033–2.38	0.57–7.69
298	1.80–12.14	4.64–11.69	179.6–1273.3	0.278–1.19	0.842–4.39	0.714–1.995	0.40–8.06	0.208–1.52	~0.017[b]–0.94	0.45–4.69
333	1.56–17.45	4.02–18.67	353.4–2842.9	0.360–0.94	1.69–4.38	1.11–1.67	0.50–10.85	0.157–1.42	~0.015[b]–1.09	1.25–10.95
368	1.36–15.35	3.56–15.24	121.5–1243.8	0.402–0.92	2.01–4.44	1.13–3.09	0.30–7.30	0.044–1.21	~0.01[b]–0.97	0.65–5.75

[a] See corresponding footnotes for Table II.

Table IV. Measured Rate Constants k (cm^3/(molecule·s))

T, K	$k_6 \times 10^{14}$	$k_7 \times 10^{12}$	$k_{8a} \times 10^{12}$
243	49.46 ± 1.64	4.07 ± 0.15	2.92 ± 0.26
268	19.12 ± 1.89	3.30 ± 0.14	3.16 ± 0.19
298	7.63 ± 0.12	2.70 ± 0.20	2.91 ± 0.09
333	2.86 ± 0.07	2.29 ± 0.12	2.98 ± 0.07
368	1.44 ± 0.26	1.90 ± 0.12	2.92 ± 0.13
			av 2.98 ± 0.11

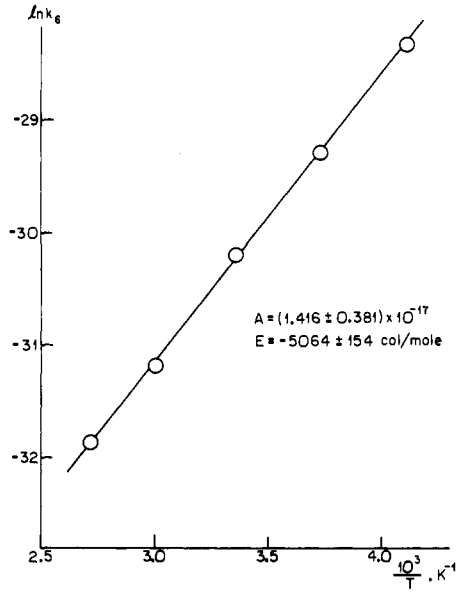

Figure 11. Arrhenius plot of k_6 (cm^3/molecule·s).

steady-state concentrations are listed in Table III at each temperature. The overall pressure ranges in the reactor cell, including that of helium diluent, are also given in the last column of Table III.

The lowest H_2O_2 concentrations in Table III were obtained from experiments with the shortest residence time (Φ_5 orifice) at low O_2 concentration. They were measured with 40-eV energy, but their uncertainty exceeds ±50%, therefore, ΔI_{34} values corresponding to H_2O_2 concentrations below 2×10^9 molecules/cm^3 were not used in calculations of k_7, k_{8a}, and k_9.

Apart from the temperature-independent rate constant k_9, Table IV summarizes the values of rate constants k_6, k_7, and k_{8a} obtained over the temperature range 243–368 K. k_{8a} is actually independent of temperature within the precision of measurements, while both k_6 and k_7 decreased with increasing temperature. The Arrhenius plot of k_6 presented in Figure 11 indicates that the temperature dependence is well described with a negative activation energy:

$$k_6 \text{ (cm}^3\text{/molecule·s)} = (1.42 \pm 0.38) \times 10^{-17} \exp[(5064 \pm 154)/RT]$$

Similarly, the Arrhenius plot of k_7 in Figure 12 also gives a negative but lesser activation energy (cal/mol):

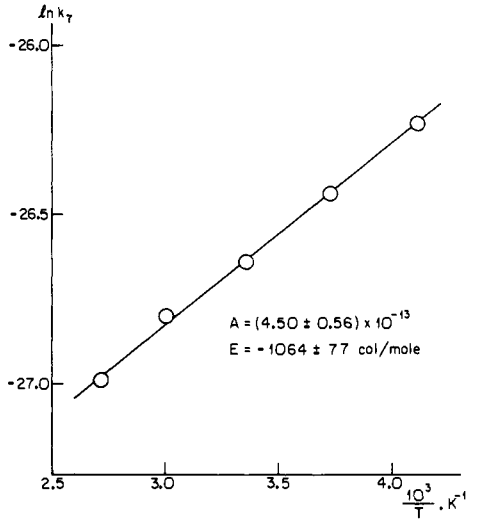

Figure 12. Arrhenius plot of k_7 (cm^3/molecule·s).

$$k_7 \text{ (cm}^3\text{/molecule·s)} = (4.50 \pm 0.56) \times 10^{-13} \exp[(1064 \pm 77)/RT]$$

Discussion

A. HO_2 Formation. The negative temperature dependence of k_6 indicates that the ethyl radical oxidation is a complex multistage process proceeding through at least two energized intermediates were the "equilibrium" of the O_2 addition step, K_a, determines the relatively slow rate of final product formation. This first step "equilibrium" seems to hold true throughout the entire temperature range explored. The direct H metathesis (a′) has a positive activation energy of about 5 kcal/mol estimated from high-temperature measurements,[23] and this reaction is the source of a combustion mechanism change above 700 K.[9] At low temperature $k_a \gg k_{a'}$, and at low pressure, where no significant $C_2H_5OO^\bullet$ stabilization takes place, a similar inequality holds true for the ethylene formation by the reaction a path, $K_a k_b \gg k_{a'}$.

An intensive search for the $m/e = 44$ signal above the normal CO_2 background showed no ethylene oxide production. Similarly, $m/e = 17$ has given no indication of OH above background. As OH is a highly reactive radical producing water in most cases, the $m/e = 18$ signal was also checked and showed no increase over the H_2O background spectrum.

Lately, reactions c and d of Scheme I have become the subject of some dispute.[4,25] Walker et al. propose[25] that the main path of C_2H_4OOH decomposition is reaction d. They studied the reaction of HO_2 with C_2H_4,[26] generating HO_2 via the thermal

(23) Cooke, D. F.; Williams, A. *Thirteenth International Symposium on Combustion*; The Combustion Institute: Pittsburgh, 1971; p 757.
(24) Benson, S. W. *J. Chem. Phys.* **1964**, *40*, 105.
(25) McAdam, K. G.; Walker, R. W. *J. Chem. Soc., Faraday Trans. 2* **1987**, *83*, 509. Baldwin, R. R.; Pickering, I. A.; Walker, R. W. *J. Chem. Soc., Faraday Trans. 1* **1980**, *76*, 2374.
(26) Baldwin, R. R.; Dean, C. E.; Walker, R. W. *J. Chem. Soc., Faraday Trans. 2* **1986**, *82*, 1445.
(27) The heat of the ethyl hydroperoxide radical is calculated from the bond energy difference of $BDE(C_2H_5\text{–}H) = 100.5$ kcal/mol and $BDE(C_2H_5\text{–}OO\text{–}H) = 88.5$ kcal/mol as $DH_f(C_2H_4OOH) = DH_f(C_2H_5OO^\bullet) + 12.0$ kcal/mol (see refs 4, 9, and the following: Kondo, O.; Benson, S. W. *J. Phys. Chem.* **1984**, *88*, 6675).
(28) Giguere, P. A. *J. Phys. Chem.* **1981**, *85*, 3733.

decomposition of 2,2,3,3-tetramethylbutane (TMB) at about 750 ± 40 K in the presence of O_2. The *tert*-butyl radicals formed generated HO_2 + isobutene in the presence of added C_2H_4, and they measured the production of ethylene oxide as well as the loss of TMB. Modeling the system and using earlier measured rate constants they deduced a rate constant for step –c which they decided was rate determining in forming the epoxide:

$$k_{-c} = 10^{9.5-17.1/\theta}\ \text{L/(mol·s)}$$

$$C_2H_4 + HO_2 \underset{c}{\overset{-c}{\rightleftharpoons}} CH_2CH_2O_2H \xrightarrow{d} CH_2{-}CH_2 + OH \quad (18)$$

Note that both steps in this scheme, (–c) and (d), are exothermic so that step c would have an activation energy of ΔH_c + 17.3 kcal/mol. Using $\Delta H_f(\text{'}C_2H_4O_2H) = 6$ kcal/mol and $\Delta H_{-c} = -9.0$ kcal/mol, they estimated $E_c = 26.3$ kcal/mol. This places the transition state for step c at 32.9 kcal/mol or some 4 kcal/mol higher than that for Et + O_2, the starting point in our system. Such a value is incompatible with our observations of a very negative activation energy for C_2H_4 + HO_2 production as well as the absence of the alternative product ethylene oxide. Our own $\Delta H_f(C_2H_4O_2H)$ estimate is 9.6 kcal/mol.[27]

To reconcile the overall negative temperature coefficient of the C_2H_5 + O_2 reaction with reaction 18d, Walker suggested[25,26] a five-member heterocyclic intermediate for the direct H metathesis which would be indistinguishable from the TS of reaction step b in Scheme I. However, such a direct process will not have a negative activation energy.

RRKM calculations[4,14] give the third-order low-pressure-limit rate constant $k^o_6 \sim 6 \times 10^{-29}$ cm^6/(molecule^2·s) for the C_2H_5 consumption rate in oxidation at 298 K. Extrapolating to the pressure range of our experimental system, the low-pressure bimolecular rate is less by one to two orders of magnitude than our measured value of k_6. It is not expected that extrapolation for an exponential function from a relatively narrow pressure range of 1–8 Torr down to 10^{-3} Torr would be accurate, but the consequence of the low k^o_6 value is that the C_2H_4 yields are overestimated at low pressures.[4,16] Such a discrepancy was noted by Gutman et al.,[4] who warned that their calculated limit pressure rate coefficients are rather RRKM fitting parameters than actual limit rate constants (see last section on Conclusions).

B. HO_2 Disproportionation. Reaction 6 produces HO_2 radicals that then are partly converted to H_2O_2 product. The H_2O_2/HO_2 distribution is the outcome of the three parallel elementary processes identified in our reaction system. H_2O_2 is produced by reactions 7 and 8a. Because of its practical importance, the bimolecular disproportionation of HO_2 is an extensively studied reaction with experiments using different HO_2 sources and both UV and IR, as well as laser magnetic resonance analytical techniques. The relatively strong negative temperature dependence of k_7 is unlikely for radical disproportionation reactions, but it can be accounted for by a hydrogen-bonded $(HO_2)_2$ equilibrium of 4-, 5-, or 6-member-ring-type short lived excited TS complex, where the 6-member-ring complex with nearly colinear hydrogen bonds is preferred.[28,39] This cyclic complex formation can be retarded with hydrogen bond forming additives, such as water,[29,30] ammonia[31] and ethanol,[32] enhancing thereby the rate of HO_2 disporportionation. The negative temperature dependence of k_7 vanishes at around 800 K and an upward turn is obtained from shock wave experiments[33] giving 12 kcal/mol activation energy for the temperature range of 750–1120 K, a surprising and uniquely strong positive temperature dependence for radical disproportionation. (**Note Added in Proof**: If the reaction is instead $2HO_2 \rightarrow 2OH + O_2$ then $\Delta H_r = 11.8$ kcal and the high E_{act} is understandable.

The known pressure dependence of this rate constant between 100 and 760 Torr is even more complex.[34] The latest data evaluation[35] gives a generalized equation of

$$k_7(M,T) = 2.3 \times 10^{-13} \exp[(1200 \pm 400)/RT] + 1.7 \times 10^{-33}(M) \exp[(2000 \pm 800)/RT] \quad (19)$$

for the combined temperature and pressure function. At millitorr and even torr pressure ranges, the termolecular contribution is negligible, therefore, our results can only be related to the first term of general eq 19. While our activation energy value agrees well with the reported value of –1.2 ± 0.4 kcal/mol, our preexponential is nearly double, and consequently, our rate constants are 55% higher than those obtained from eq 19 throughout the temperature range of our experiments and they are rather close to $k_7(M,T)$ values at 1 atm of pressure. Also, our Arrhenius function shows excellent agreement with that of Patrick and Pilling[36] and a good correlation with that of Lightfoot et al.[37] Both have studied reaction 7 at 760 Torr of pressure.

One possible explanation of the joint negative temperature and positive pressure dependences involves the excited and collisionally stabilized $(HO_2)_2$ equilibrium:[38]

$$HO_2 + HO_2 \underset{a}{\overset{a}{\rightleftharpoons}} (HO_2)^*_2 \xrightarrow{b} H_2O_2 + O_2 \quad (20)$$

$$(HO_2)^*_2 \underset{c}{\overset{(M)}{\rightleftharpoons}} (HO_2)_2$$

where the zero-pressure contribution arises from reaction paths a, –a, and b, the mechanism expected to prevail in our millitorr pressure system. This scheme was applied to a two-channel RRKM modeling with linear tetroxide and varied thermochemical data of the $(HO_2)_2$ TS complex,[29,38] as well as the 6-member cyclic hydrogen-bonded dimer TS.[39] No satisfactory unified description could be obtained from those model calculations when the deuterium isotope effect and rate enhancement by polar additives were also considered. Reaction scheme 20 might be more complex if a product channel of $(HO_2)_2 \rightarrow H_2O_2 + O_2(^1\Delta_g)$ would be demonstrated.

While there is nearly general agreement on the value of k_7 at 298 K and 760 Torr of pressure, the pressure dependence given by eq 19 is controversial. Using the molecular modulation/UV absorption technique, Cox and Burrows[40] found no pressure dependence between 25 and 760 Torr, but some fall-off between 3 and 10 Torr of pressure which might be an artifact since it is partly compensated by the decrease in the UV absorption cross section observed at low pressures.[40] Besides extrapolation between 100 and 760 Torr of pressure, the zero pressure value of k_7 is also obtained from low-pressure IR absorption[41] and laser magnetic resonance technique[42,43] (1–20 Torr) measurements where the contribution of the termolecular term is small. Those results show a scatter[42] of (1.4–2.1) × 10^{-12}, the same as given by eq 19, and some sensitivity to surface treatment of the reactor vessel.[43]

(29) Kircher, C. C.; Sander, S. P. *J. Phys. Chem.* **1984**, *88*, 2082.
(30) DeMore, W. B. *J. Phys. Chem.* **1979**, *83*, 1113.
(31) Hamilton, E. J.; Lii, R. R. *Int. J. Chem. Kinet.* **1980**, *9*, 875. Lii, R. R.; Gorse, R. A.; Sauer, M. C.; Gordon, S. *J. Phys. Chem.* **1980**, *84*, 813.
(32) Anderson, B. Y.; Cox, R. A.; Jenkin, M. E. *Int. J. Chem. Kinet.* **1988**, *20*, 283.
(33) Hippler, H.; Troe, J.; Willner, J. *J. Chem. Phys.* **1990**, *93*, 1755.
(34) Sander, S. P.; Peterson, M.; Watson, R. T. *J. Phys. Chem.* **1992**, *86*, 1236. Kurylo, M. J.; Quellette, P. A.; Laufer, A. H. *Ibid.* **1986**, *90*, 437. Simonaitis, R.; Heicklen, J. *Ibid.* **1982**, *86*, 3416.
(35) DeMore, W. B.; Sander, S. P.; Golden, D. M.; Hampson, R. F.; Kurylo, M. J.; Howard, C. J.; Ravishankara, A. R.; Kolb, C. E.; Molina, M. J. NASA Evaluation No. 10, *Chemical Kinetics and Photochemical Data for Use in Stratospheric Modeling*; JPL Publication 92-20, 1992.
(36) Patrick, R.; Pilling, M. J. *Chem. Phys. Lett.* **1982**, *91*, 343.
(37) Lightfoot, P. D.; Veyret, B.; Lesclaux, R. *Chem. Phys. Lett.* **1988**, *150*, 120.
(38) Patric, R.; Barker, J. R.; Golden, D. M. *J. Phys. Chem.* **1984**, *88*, 128.
(39) Mazurkewich, M.; Benson, S. W. *Int. J. Chem. Kinet.* **1985**, *17*, 787.
(40) Cox, R. A.; Burrows, J. P. *J. Phys. Chem.* **1979**, *83*, 2560.
(41) Thrush, B. A.; Tyndall, G. S. *J. Chem. Soc., Faraday Trans. 2* **1982**, *78*, 1469.
(42) Rosenstein, V. B.; Gershenzon, Y. M.; Il'in, S. D.; Kiskovitch, O. P. *Chem. Phys. Lett.* **1984**, *112*, 473.
(43) Takacs, G. A.; Howard, C. J. *J. Phys. Chem.* **1984**, *88*, 2110. Takacs, G. A.; Howard, C. J. *Ibid.* **1986**, *90*, 687.

So far, the disproportionation rate constant k_7 was exclusively obtained by measuring the rate of HO_2 consumption. HO_2 radical generation requires a complex photochemical system of at least three initial components where a relatively large number of reactions (usually of 15–20) has to be considered. The hydroperoxyl radical consumption rate then gives k_{obs}/σ, where σ is the absorption cross section at the applied wavelength and k_{obs} is the observed rate constant. With this method, k_{obs} and σ are actually interdependent variables. Under proper kinetic conditions $k_{obs} \simeq k_7$, and with pure second-order kinetics $\sigma = \sigma_{HO2} - {}^1/_2\sigma_{H2O2}$. No allowances are made for UV absorptions of organic or organic peroxy radicals even for the $(HO_2)_0$ concentration in the $Cl_2/CH_3OH/O_2$ hydroperoxyl radical generating system.[34,36,37] Also, pure second-order removal of HO_2 was assumed in the light-off period of photolysis. However, the $Cl_2/CH_3OH/O_2$ system of hydroperoxyl radical generation may be perturbed by first-order HO_2 consumption reactions, especially at low (<1 Torr) pressure.[44] The photochemical $Cl_2/H_2/O_2$ hydroperoxyl radical generating kinetic system of molecular modulation[45] also follows the decrease of k_7 with pressure according to eq 19 when only the second-order removal of HO_2 radicals is taken into account, but it is shown qualitatively that the first-order removal tends to increase with decreasing pressure in this system.[40] Along with considerable wall reaction[46] of HO_2, such first-order consumption may come from reaction 9 and the reaction $HO_2 + H \rightarrow 2HO$ in the $Cl_2/H_2/O_2$ photochemical system.

Partial decomposition of H_2O_2 by low-power electric discharge in a low-pressure (0.6 Torr) flow system also produces HO_2 radicals. The second-order time dependent disappearance of HO_2 radicals,[47] measured by absolute mass spectrometric analysis, gives $k_7 = 3 \times 10^{-12}$ cm^3/(molecule·s) at 298 K, which is in good agreement with our result.

Since eq 19 is mainly derived from data at 1–760 Torr of pressure and the experimental pressure dependence is not satisfactory, the high pressure data of k_7 may be of interest. The electron pulse radiolysis of the H_2/O_2 system at 1.5 and 2 atm of pressure using time-dependent UV absorption of HO_2 analysis[48] gives the same value for k_7 at 298 K as the above photokinetic methods at 1 atm.

In our experimental system, the steady-state concentrations of *both* HO_2 and H_2O_2 are measured along with the rate of hydroperoxyl radical formation. Reactions 6–9 fully account (±4%) for HO_2 and H_2O_2 mass conservation. The bimolecular disproportionation rate of HO_2 radicals is best controlled with residence time (exit orifice size) change.

C. Ethyl + HO_2 Disproportionation. Depending on the concentration of reactants and the residence time, the contribution of reaction 8a to H_2O_2 formation varies between 6.5 and 85%. This large variation makes possible the accurate determination of k_{8a}. This is an important step in complex oxidation and atmospheric processes. k_{8a} is known so far from a low-value estimate[20] which would render reaction 8a negligible in most cases. However, this is not so here. Its competition with reaction 7 can be well-demonstrated in our system by using the exit orifice changeover. The kinetics of reactions 8a and 8b cannot be separated experimentally. The assumption that $k_{8a} \sim k_{8b}$ is based on the near equality of heats of reactions of both processes.[20] Baldwin[49] et al. also gives an estimate of $k_{8b} \sim 10^{-11}$–10^{-12} cm^3/(molecule·s). Any significant difference between k_{8a} and k_{8b} would contribute doubly to the calculation of k_9 according to eqs 12b and 16 and we should be able to observe its influence.

Table V. Rate Constants Reported for the Cl + HO_2 Reaction at 298 K[a]

$k_9 \times 10^{11}$ cm^3/(molecule·s)	method	ref
5.9 ± 2.9[a]	relative	56
3.5 ± 1.5[a]	relative	57
6.8 ± 2.5	relative	58
4.4 ± 0.5[a]	relative	59
5.3 ± 1.7	UV/MM	60
4.2 ± 0.7	IR/MR	61
4.45 ± 0.06	VLPR	this work

[a] Rate constants of the reference reaction rate updated according to ref 35. MM = molecular modulation. MR = magnetic resonance.

The most unexpected result of our studies lies in the absence of any observable species containing carbon and oxygen. It is expected that the predominant product of the $C_2H_5 + HO_2$ reaction would be recombination to produce excited $(C_2H_5OOH)^*$. This intermediate would have an excitation energy of 71 kcal/mol arising from the newly formed bond[50] and it has three competing paths for decomposition:

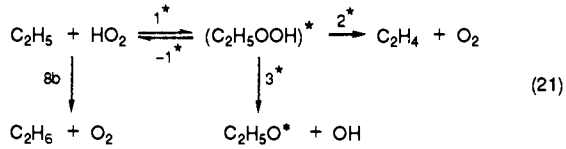

(21)

The fastest of these three paths is expected to be reaction 3* with an A factor of about 2.8×10^{15} s^{-1} and a barrier of 43 kcal/mol.[10] We see no evidence of such a path, meaning that less than 5×10^9 molecules/cm^3 of either OH or $C_2H_5O^\cdot$ are produced. Our only explanation for these observations is that energy relaxation does not occur on a time scale comparable to that needed for reaction 3*. A similar astonishing result has been found for ethyl radical recombination.[18,51]

D. Cl + HO_2 Interaction. In spite of the relatively low concentration of Cl atoms, reaction 9 plays a significant part in hydroperoxyl radical consumption. Since reaction 9b is slightly endothermic, the main component of the total rate constant is expected to be k_{9a} in our temperature range. The unusually high value of k_{9a} can be understood by a "contact" transition state mechanism[52] proposed for alkyl radical disproportionation and also applied to C_2H_5 + Cl disproportionation.[18]

The total rate constant k_9 obtained from Cl and HO_2 consumption rates is in good agreement with known values measured in a variety of kinetic systems using relative rate studies in relation to Cl + H_2 reaction[53] and Cl + H_2O_2 reaction[53–56] as well as with absolute rate measurements using UV absorption molecular modulation[57] (under the bimolecular condition of Cl and HO_2 consumption rate) and laser magnetic resonance[58] (under the conditions $[Cl] \gg [HO_2]$) techniques. Relevant rate constant data are presented for comparison in Table V.

While there is a nearly general agreement on the value of k_9 in the literature, the branching of k_{9b}/k_9 varies: ~ 0.01[56] to 0.17[57] and 0.22.[58] Reaction 9 is a fundamental step in atmospheric chemistry as it accounts for nearly 50% of a temporary sink for active Cl atoms at stratospheric altitudes. The branching ratio is thus an important factor to the extent that it is a termination (reaction 9a) or instead produces two new reactive intermediates

(44) Grotheer, H. H.; Riekert, G.; Meier, U.; Just, T. *Ber. Bunsenges. Phys. Chem.* **1985**, *89*, 187.
(45) Crowley, J. N.; Simon, F. G.; Burrows, J. P.; Moortgat, G. K.; Jenkin, M. E.; Cox, R. A. *J. Photochem. Photobiol. A: Chem.* **1991**, *60*, 1.
(46) Howard, C. J. *J. Phys. Chem.* **1979**, *83*, 3. Cantrell, C. A.; Stedman, D. H.; Wendel, G. J. *Anal. Chem.* **1984**, *56*, 1496.
(47) Foner, N. S.; Hudson, R. L. *Adv. Chem. Ser.* **1962**, *36*, 34.
(48) Lii, R. R.; Gorse, R. A.; Sauer, M. C.; Gordon, S. *J. Phys. Chem.* **1980**, *84*, 813. Hamilton, E. J.; Lii, R. R. *Int. J. Chem. Kinet.* **1977**, *9*, 875.
(49) Baldwin, R. R.; Walker, R. W. *Trans. Faraday Soc.* **1969**, *65*, 806.
(50) Benson, S. W.; Nangia, P. S. *Acc. Chem. Res.* **1979**, *12*, 223.
(51) Benson, S. W.; Dobis, O.; Gonzales, A. C. *J. Phys. Chem.* **1991**, *95*, 8423.
(52) Benson, S. W. *Can. J. Chem.* **1983**, *61*, 881. Benson, S. W. *J. Phys. Chem.* **1985**, *89*, 4366.
(53) Cox, R. A. *Int. J. Chem. Kinet.* **1980**, *12*, 649.
(54) Leu, M. T.; DeMore, W. B. *Chem. Phys. Lett.* **1976**, *41*, 121.
(55) Poulet, G.; Le Bras, G.; Combourieu, J. *J. Chem. Phys.* **1978**, *69*, 767.
(56) Burrows, J. P.; Cliff, D. J.; Harris, G. W.; Thrush, B. A.; Wilkinson, J. P. T. *Proc. R. Soc. London* **1979**, *A368*, 463.
(57) Cattell, F. C.; Cox, R. A. *J. Chem. Soc., Faraday Trans. 2* **1986**, *82*, 1413.
(58) Lee, Y. P.; Howard, C. J. *J. Chem. Phys.* **1982**, *77*, 756.

(reaction 9b) in the stratospheric Cl cycle. For this reason, any small increase of $m/e = 51$ mass signal over the background was carefully analyzed in our experiments.

Estimating the mass spectrometric efficiency of ClO as $\alpha_{51} = 6.4 \times 10^{-11}$ from those of O_2 and Cl_2 at 40-V ionization potential, the scatter of $m/e = 51$ background signal sets the sensitivity limit of our analytical method to $F(ClO) = 7.4 \times 10^9$ molecules/(cm^3·s). At 20 V mass spectrometry, this limit is 3×10^{10} molecules/(cm^3·s). The only chemical reaction for ClO in our system is

$$ClO + HO_2 \rightarrow HOCl + O_2 \qquad (22)$$

$$k_{22} = 5 \times 10^{-12}\ cm^3/(molecule{\cdot}s)^{35}$$

With this addition to our Scheme III, the rate constant of reaction 9b can be calculated as

$$k_{9b} = \frac{F(ClO)}{(Cl)}\left[\frac{1}{(HO_2)} + \frac{k_{22}}{k_{eClO}}\right] \qquad (23)$$

where $F(ClO)$ is calculated from the relatively small increase (at 40 eV) of $m/e = 51$ mass signal over the background measurable in those runs where $(HO_2) > 1 \times 10^{11}$ molecules/cm^3 and $(C_2H_5) < 1 \times 10^{11}$ molecules/cm^3. The rate constant values individually calculated with eq 24 cover a range from 1×10^{-12} to 5.2×10^{-12} cm^3/(molecule·s) with the statistical average of $k_{9b} = (2.2 \pm 1.4) \times 10^{-12}$ cm^3/(molecule·s) No temperature dependence exceeding this large scatter can be assigned. This value sets the branching ratio of reaction 9 to $k_{9b}/k_9 = 0.05 \pm 0.03$ which is considerably less than the value suggested by the latest data evaluation[35] and is rather close to the low value of Burrows et al.[56]

For more accurate measurements higher reactant concentrations, especially a higher Cl concentration, would be needed to attain significant ClO formation, but our complex system, mainly because of the fast reaction 2 in Scheme II, is not suited to that condition. On the other hand, ClO is a reactive intermediate which can be lost in a number of other radical reactions, as well as formed by the two-step $2Cl + O_2 + M$ reaction in a more complex and higher pressure system.[59] Influences of such complexities can be found in the work of Lee and Howard.[58] While their overall rate constant k_9, measured under the $(Cl) \gg (HO_2)$ kinetic condition, is in an excellent agreement with our value, omitting reaction 22 and using a 33% lower rate constant for ClO formation by the reaction Cl + ClOO (the updated rate constant is 1.2×10^{-11} cm^3/(molecule·s),[35] instead of the value they used, 8×10^{-12} cm^3/(molecule·s)) led to an overestimate for k_{9b} from measurements of ClO production.

An even greater problem of that work[58] arises from the operation of the forechamber used for the preparation of HO_2 and connected to the reaction flow tube through a capillary inlet constriction. This forechamber may produce up to 25% of HO_2 by reaction 7 of Scheme III. Consequently, some extra HO_2 will be produced by the reaction

$$Cl + H_2O_2 \rightarrow HO_2 + HCl \qquad (24)$$

$$k_{24} = 4.1 \times 10^{-13}\ cm^3/(molecule{\cdot}s)$$

which then makes the contribution of $2k_{9b}(Cl)t(H_2O_2)_o/(HO_2)_o$, where t is the reaction time, to k_{9b}/k_9 values when they are calculated from the measured $(OH)_t/(HO_2)_o$ or $(ClO)_t/(HO_2)_o$ ratios. Taking $(H_2O_2)_o/(HO_2)_o = 0.25$ and $(Cl)t = (1.5\text{–}2.0) \times 10^{11}$ corresponding to the experimental conditions, the branching ratio is reduced to between 0.045 and 0.035, about the same as given by our measurements. At the same time, this extra HO_2 production negligibly increases the k_9 value (by less than 1%), but it eliminates the approximately 10% deficiency between $(HO_2)_o$ and $(HO_2)_{z\rightarrow 0}$ in the original data evaluation, where z (cm) is the reaction zone length of the flow tube (see Figure 4 of ref 58). Actually this gap was the starting point for the estimation of the 25% (H_2O_2) contamination in the inlet flow of $(HO_2)_o$.

A similar overestimate of k_{9b} can be traced in the more complex UV photolytic system of Cattel and Cox,[57] where the simulation with uncorrected steady-state Cl concentrations established by the light-on period gives k_9 higher by 40% than our value, but 0.07 for the k_{9b}/k_9 branching ratio. They made an arbitrary 40% decrease of $(Cl)_{ss}$ for the flash period which then reduces k_9 to an acceptable value, but increases k_{9b} by a factor of 2.5. However, a simple update of rate constants[35] for reactions Cl + O_2 + M and Cl + ClOO in their mechanism used in computer simulation would result in nearly the same reduction of the k_9 value without significant change in the branching ratio of 0.07.

Reaction 9b is reversible. However, reaction –9b has two competing channels, reproducing HO_2 + Cl products in a ratio of 86–98%,[62,63] while the rest takes the minor channel of HCl + O_2. The endothermicity of reaction 9b is either 2.2 or 1.7 kcal/mol depending upon whether 2.5 kcal/mol[20,60] or 3.0 kcal/mol[61] is taken for the standard heat of HO_2 radical formation. Those two reaction enthalpy values give the equilibrium constant $K_{9b} = 0.18$ or 0.41, indicating that the backward reaction is faster than the forward reaction at room temperature.

Two investigations of the back reaction[62] in the discharge-flow system under the condition $(ClO) \gg (OH)$ give the rate constant $k_{-9b} = (1.85 \pm 0.13) \times 10^{-11}$ cm^3/(molecule·s) at 298 K. One of them[62a] uses a five times higher rate constant for the Cl + ClO_2 reaction (ClO source) than the currently accepted value (1.2×10^{-11}, cm^3/(molecule·s)[35]). Their other common method of ClO generation is from Cl + $O_3 \rightarrow$ ClO + O_2 under the condition $(O_3) > (Cl)$. Since the excess O_3 removes the Cl atom formed in reaction –9b

$$OH + ClO \xrightarrow{-9b} HO_2 + Cl$$

the other product can now be removed by the HO_2 + OH reaction. However, its rate constant is 72% higher (1.1×10^{-11} cm^3/(molecule·s)[35]) than that used in their reaction scheme for computer simulation. This rapid removal of OH can account for the overestimate of k_{-9b} by about a factor of 2.

The other three works[63] are mainly free from the above methodological inadequacies and they give an average value of $k_{-9b} = (1.09 \pm 0.16) \times 10^{-11}$ cm^3/(molecule·s). Combining this value with the above equilibrium constant K_{9b} and taking account of a 86% reversibility, $k_{-9b} = 1.7 \times 10^{-12}$ or 3.8×10^{-12} cm^3/(molecule·s) is obtained which then sets the branching ratio of reaction 9 to between 0.038 and 0.085. This is not better than our experimental observation, but it supports the branching ratio of k_{9b}/k_9 being as low as 0.05–0.06 at room temperature.

Conclusions

The present experimental study demonstrates that the VLPR system has outstanding features for application to such complex kinetic measurement as the low-pressure oxidation of organic free radicals with molecular oxygen. Varying the initial concentrations of all three reactants in a wide range as well as the residence time has provided the necessary variations of kinetic parameters to determine a number of rate constants accurately. The mass spectrometric product analysis disclosed that the reactions listed in Schemes II and III represent >95% of the relevant chemistry in the system. Thus it was possible to account for the complete kinetics with the use of only measured rate

(59) Burrows, J. P.; Cox, R. A. *J. Chem. Soc., Faraday Trans. 1* **1981**, *77*, 2465.

(60) Howard, C. J. *J. Am. Chem. Soc.* **1980**, *102*, 6937.

(61) Shum, L. G. S.; Benson, S. W. *Int. J. Chem. Kinet.* **1983**, *15*, 323. Shum, L. G. S.; Benson, S. W. *Ibid.* **1983**, *15*, 341.

(62) (a) Poulet, G.; Leverdet, G.; Le Bras, G. *J. Phys. Chem.* **1986**, *90*, 159. (b) Hills, A. J.; Howard, C. J. *J. Chem. Phys.* **1984**, *81*, 4458.

(63) Ravishankara, A. R.; Eisele, F. L.; Wine, P. H. *J. Chem. Phys.* **1983**, *78*, 1140. Burrows, J. P.; Wallington, T. J.; Wayne, R. P. *J. Chem. Soc., Faraday Trans. 2* **1984**, *80*, 957. Leu, M. T.; Lin, C. L. *Geophys. Res. Lett.* **1979**, *6*, 425.

constants. With respect to overall product analysis, the simultaneous measurements of ethyl radical consumption and ethylene formation, as well as of HO_2 and H_2O_2 distribution, provide cross-checks of the kinetics.

The four-step oxidation mechanism proposed in Scheme I contains several collisional stabilization steps which would make the entire kinetics pressure dependent. Those steps are apparently absent in our millitorr pressure system for lack of effective third-body collisions.

It will be of interest to make an RRKM model for steps a, b, and c of Scheme I. Our data which suggest that step b is rate determining will make it possible to fix the ratios of ΔH°_a to the activation energy E_b of step b. This and the apparent absence of pressure effects in reaction 7 will be dealt with in a forthcoming paper.

One of the most surprising results of our study, similar in some respect to the absence of butane in the Cl/C_2H_6 system,[18] is the apparent slowness of $C_2H_5 + HO_2$ recombination. As before it must be attributed to a slowness of energy relaxation[51] in the energized adduct $C_2H_5O_2H^*$.

Acknowledgment. This work has been supported by a grant from the National Science Foundation (CHE-87-1467).